

Magnetic anisotropy effects on quantum impurities in superconducting host

Rok Žitko^{1,2}, Oliver Bodensiek³, Thomas Pruschke³

¹ *Jožef Stefan Institute, Jamova 39, SI-1000 Ljubljana, Slovenia,*

² *Faculty of Mathematics and Physics, University of Ljubljana, Jadranska 19, SI-1000 Ljubljana, Slovenia,*

³ *Institute for Theoretical Physics, University of Göttingen, Friedrich-Hund-Platz 1, D-37077 Göttingen, Germany*

(Dated: November 2, 2018)

We study the magnetic anisotropy effects on the localized sub-gap excitations induced by quantum impurities coupled to a superconducting host. We establish the ground-state phase diagrams for single-channel and two-channel high-spin Kondo impurities; they unveil surprising complexity that results from the (multi-stage) Kondo screening in competition with the superconducting correlations and the magnetic anisotropy splitting of the spin multiplets. We discuss the possibility of detecting the Zeeman splitting of the sub-gap states, which would provide an interesting spectroscopic tool for studying the magnetism on the single-atom level. We also study the problem of two impurities coupled by the Heisenberg exchange interaction, and we follow the evolution of the sub-gap states for both antiferromagnetic and ferromagnetic coupling. For sufficiently strong antiferromagnetic coupling, the impurities bind into a singlet state that is non-magnetic, thus the sub-gap states move to the edge of the gap and can no longer be discerned. For ferromagnetic coupling, some excited states remain present inside the gap.

PACS numbers: 72.10.Fk, 72.15.Qm, 73.20.Hb, 73.20.-r

I. INTRODUCTION

Tunneling spectroscopy is the prevalent experimental approach for studying superconductivity. It provides information on such fundamental properties as the energy gap, pairing symmetry, and pairing interactions^{1–6}. Using a scanning tunneling microscope (STM) it is possible to examine the impurity effects on the single-atom level^{4,7–18}; see Fig. 1a). Such measurements provide crucial data on the nature of the superconducting state in complex materials^{3,5}. With improvements in the instrumentation, experiments are being performed at increasingly low temperatures and ever further details in the local density of states (LDOS) can be resolved: recent STM work performed in the 300 mK range on magnetic adatoms adsorbed on superconductors has clearly revealed the existence of multiple sub-gap excitation peaks^{19–21}; see Fig. 1b). It was proposed that these may be interpreted as the magnetic-impurity-induced bound states associated with the different angular-momentum scattering channels^{19,22,23}, but we show in this work that an alternative interpretation in terms of the magnetic-anisotropy effects is also possible.

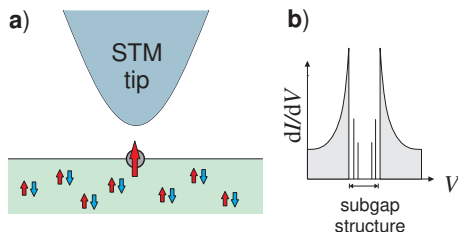


Figure 1: (Color online) (a) Magnetic impurity atom adsorbed on the superconductor surface probed by the STM. (b) Idealization of the characteristic differential conductance spectrum as recorded by the STM above a magnetic impurity: in the gap, the LDOS is essentially zero except for the discrete peaks which correspond to the transitions from the ground state to the sub-gap excited states.

Since the magnitude of the magnetic anisotropy of magnetic adsorbates is comparable or may even exceed the superconducting gap^{24,25}, its effects are drastic, yet they have received hardly any attention in this context. In addition, it has been very recently demonstrated that the strength of the anisotropy (parameter D) in magnetic molecules can be continuously tuned in mechanical break junctions²⁶; using superconducting leads, one could then directly study the effect of the magnetic anisotropy on the transport and the spectral properties of magnetic molecules coupled to superconductors. Finally, spin-orbit coupling is always present for any impurity atom embedded in the superconducting bulk, therefore the class of problems in which an anisotropic spin degree of freedom is coupled to a superconducting host is indeed wide ranging.

The theory of magnetic impurities in a superconductor was first worked out within simplified classical-spin models^{27,28}, while later works took into account the quantum nature of impurities and, among other improvements, properly described the competition between the screening of the impurity moment by the Kondo effect and the superconducting correlations²⁹. The crucial difference between a classical and quantum spin is that a classical spin is static (essentially equivalent to a local point-like magnetic field), it has no internal dynamics, and it cannot flip the spin of the conduction-band electrons. For this reason, the impurity problem in a classical-spin approximation is a non-interacting (mean-field) theory. The quantum impurity, however, needs to be treated using the tools of the many-particle theory, which can take into account the non-perturbative effects induced by strong interactions. The behavior of classical and quantum impurities is very different in many respects. For classical impurities, there is no difference if the coupling to the conduction-band electrons is ferromagnetic or antiferromagnetic, while real quantum impurities have very different properties in these two cases. Furthermore, in the absence of magnetic anisotropy,

a quantum impurity model has full $SU(2)$ spin symmetry and any breaking of this rotational invariance would indicate a deficiency of the method used; a classical spin, however, explicitly breaks the spin symmetry even at the level of the Hamiltonian itself. Unless there is a physical mechanism that can lead to a real symmetry breaking [such as spontaneous symmetry breaking due to magnetic ordering induced by inter-impurity Ruderman-Kittel-Kasuya-Yosida (RKKY) interaction], only a quantum impurity model can thus provide the qualitatively correct result, while a classical model will be affected by spurious symmetry breaking. (In magnetically-ordered systems, classical spin models may be fully adequate for many purposes.) The spin $SU(2)$ symmetry breaking also implies the breaking of the time-reversal symmetry. This has important consequences for the degeneracy of the sub-gap states (cf. Kramers' degeneracy theorem) and it is one of the major differences between quantum and classical (static) impurities. This dichotomy recently gained renewed attention in the context of topological insulators³⁰⁻³², since only impurities which break the time-reversal invariance can open the gap in the topologically-protected edge/surface states³³⁻⁴².

Accurate calculations for quantum impurities in superconductors became possible by generalizing the numerical renormalization group (NRG) method to problems with a superconducting electron bath⁴³. This method was applied to simplified models such as the spin-1/2 Kondo model⁴³⁻⁴⁵ and the non-degenerate Anderson impurity model⁴⁶. Real magnetic impurity atoms and molecules generally require, however, a more sophisticated description in terms of the multi-channel degenerate Anderson model or the high-spin Kondo model with magnetic anisotropy terms⁴⁷. The goal of the present work is thus to apply the NRG to study the sub-gap excitations for such more realistic models, featuring anisotropic high-spin Kondo impurities with more than one channel. There are some related works in the literature. Lee et al. have studied the isotropic high-spin impurities in a side-coupled configuration⁴⁸ and the two-level impurity model⁴⁹. The two-channel models have been studied in the context of unconventional superconductors⁵⁰ and iron pnictide superconductors⁵¹. Moca et al. have demonstrated the presence of multiple sub-gap states in a multi-orbital model for Mn impurity in MgB_2 ⁵². Multiple sub-gap states also appear in the case of XXZ anisotropic Kondo exchange coupling in the $S_{\text{imp}} = 1/2$ Kondo model⁴⁵. Multi-channel high-spin Kondo models with magnetic anisotropy terms, however, have not yet been studied.

The paper is structured as follows. In Sec. II, we define the model and comment on its relevance for actual adsorbate systems. In Sec. III, we study the ground state diagrams for various one- and two-channel isotropic high-spin Kondo systems, while the magnetic anisotropy effects are presented in Sec. IV. The spectral peaks and their splitting due to the magnetic anisotropy in the multi-channel case are discussed in Sec. V. Section VI is devoted to the role of the external magnetic field, which splits all many-particle states with $S \neq 0$. Finally, impurity dimers are studied in Sec. VII.

II. MODEL AND METHOD

We describe the impurity system by the Hamiltonian $H = H_{\text{band}} + H_{\text{imp}}$, where H_{band} describes N channels of conduction-band electrons using the mean-field BCS Hamiltonian with the gap Δ ⁴³:

$$H_{\text{band}} = \sum_{i=1}^N \left[\sum_{k\sigma} \epsilon_k c_{k\sigma i}^\dagger c_{k\sigma i} + \sum_k \Delta \left(c_{k\uparrow i}^\dagger c_{k\downarrow i} + \text{H.c.} \right) \right],$$

while the impurity is described by a Kondo-like Hamiltonian with a magnetic anisotropy term^{47,53-58}:

$$H_{\text{imp}} = \sum_{i=1}^N J_i \mathbf{S}_{\text{imp}} \cdot \mathbf{s}_i + D S_{\text{imp},z}^2 + g \mu_B B S_{\text{imp},z}.$$

Here J_i are the exchange coupling constants, \mathbf{S}_{imp} is the impurity spin operator satisfying the $su(2)$ Lie algebra [$S_{\text{imp},\alpha}, S_{\text{imp},\beta} = i\epsilon_{\alpha\beta\gamma} S_{\text{imp},\gamma}$], and \mathbf{s}_i is the channel- i spin density at the position of the impurity:

$$\mathbf{s}_i = \frac{1}{\mathcal{N}} \sum_{kk'\alpha\beta} c_{k\alpha i}^\dagger \left(\frac{1}{2} \boldsymbol{\sigma}_{\alpha\beta} \right) c_{k'\beta i}, \quad (1)$$

where \mathcal{N} is the number of the states in the conduction band. Furthermore, D is the longitudinal anisotropy, g is the impurity g -factor, μ_B is the Bohr magneton, and B is the external magnetic field (non-zero B is discussed in Sec. VI). The multiple channels correspond to the different symmetry channels of the Bloch states, which hybridize with the impurity d -levels; our high-spin Kondo model may be thought to arise from some multi-orbital Anderson model after performing the Schrieffer-Wolff transformation⁵⁹⁻⁶⁵. Strictly speaking, the low-energy effective model for a multi-orbital Anderson model is not necessarily a high-spin Kondo model. Such an exception occurs, for example, if the system is not in the local-moment regime, but rather its valency is strongly fluctuating, or if there is also some orbital moment on the impurity atom. For surface-adsorbed impurities, the symmetry in real space is broken, thus it is reasonable to expect strong quenching of the orbital moment. The valence-fluctuation regime cannot be excluded a priori, but the systems of such complexity are beyond the capabilities of the NRG method. In this work we thus focus on the problems where the orbital moment is quenched and the electrons in the d -orbitals are locked into a high-spin state by the strong Hund's coupling. Such cases are adequately described by the proposed model. For $D \neq 0$ or $B \neq 0$, the Hamiltonian only has an axial $U(1)$ spin symmetry, thus the sole conserved quantum number is S_z , the z component of the total spin.

The NRG method consists of discretizing the continua of the conduction-band states, rewriting the Hamiltonian in the form of one-dimensional tight-binding chains with an exponentially decreasing hopping constants, and diagonalizing the resulting Hamiltonian iteratively by adding one further chain site per channel in each step⁶⁶⁻⁶⁸. The spectrum of many-particle states is truncated to the low-energy part after each

step. Due to the low symmetry of the problem (there is no particle conservation in the superconducting case, and there is only partial spin symmetry in the presence of magnetic anisotropy or magnetic field), these calculations are numerically very demanding. The size of the matrices that need to be diagonalized at the given truncation cutoff strongly depend on the value of the discretization parameter Λ . In many situations, one can use a large value of Λ and reduce the discretization artifacts by the so-called z -averaging trick^{69–73}; this approach produces excellent results for featureless (flat) conduction bands. One needs to be very careful, however, in the vicinity of phase transitions, since the ground state obtained in a calculation can be z -dependent (in other words, it is possible that for exactly the same model parameters, one obtains a different ground state for different interleaved discretization meshes). The averaging may then be ill-defined for an interval of parameters where such z -dependence of the ground state occurs. The width of this interval grows as Λ is increased. Nevertheless, experience shows that in spite of this difficulty, one can determine the transition point very accurately even by performing the calculations with a very large value of Λ . Test calculations on simple problems, for example, show that by determining the value of the system parameter where the transition occurs for a fixed value of z , and averaging such results over z , one obtains a value that changes little with Λ . Often it is sufficient to use only two values of z (such as 1 and 0.5) to obtain good results. This approach has been used, for example, to establish the accurate values tabulated in Table I in the following section. In other parts of this work, where high accuracy was not essential, we performed no such averaging, thus the results are only qualitatively correct.

III. TRANSITIONS IN THE ISOTROPIC MODEL

The properties of the multi-channel Kondo model in the normal state depend on the relation between the number of channels and the impurity spin; roughly speaking, each channel can screen one half unit of the impurity spin^{65,74–80}. Thus, for $N < 2S_{\text{imp}}$, the impurity spin can be only partially screened, while for $N = 2S_{\text{imp}}$ there is an exact spin compensation, yielding a singlet ground state (GS); for $N > 2S_{\text{imp}}$, exotic non-Fermi-liquid (NFL) states may arise⁸¹. In the superconducting state, the behavior of the Kondo model is only well explored for the simplest case of $N = 1$ and $S_{\text{imp}} = 1/2$ ⁴³: as the gap Δ is increased from zero, there is a transition at Δ_c between the regime where the impurity is Kondo-screened (singlet ground state) to the regime where the impurity is free (doublet ground state). The value of Δ_c is of the order T_K , the Kondo temperature, which is the characteristic energy scale of the Kondo effect. The transition occurs because in the superconducting state there is an insufficient number of low-energy electron states to participate in the Kondo screening.

We now consider the general multi-channel high-spin case, first in the absence of the anisotropy and for equal coupling constants J_i for all channels. By analogy with the known results, we expect that for $2S_{\text{imp}} \geq N$ there is a transition from

the Kondo screened $S = S_{\text{imp}} - N/2$ state to the “free-spin” $S = S_{\text{imp}}$ state as the gap is increased. Our NRG calculations fully support this picture. For $2S_{\text{imp}} < N$ the NFL effects make a-priori predictions difficult; in numerical simulations for $N = 2$ and $S_{\text{imp}} = 1/2$, we observe a transition from a degenerate pair of singlet states to a doublet ground state as Δ increases. The Δ_c for $N = 1$ and $N = 2$ are tabulated in Table I for a range of S_{imp} . The ratio Δ_c/T_K strongly depends on S_{imp} in spite of the fact that the superexchange couplings are constant and thus the Kondo scale is formally the same in all cases. The variation with N is weaker, with a notable exception of the NFL case with $N = 2$, $S_{\text{imp}} = 1/2$, where Δ_c/T_K is much reduced.

S_{imp}	1/2	1	3/2	2	5/2
$N = 1$	3.7	5.9	10.3	19.8	43
$N = 2$	0.70	5.7	11.3	23	51

Table I: Dependence of the ratio Δ_c/T_K between the critical gap and the Kondo temperature on the number of channels N and the impurity spin S_{imp} . In the two-channel case, the coupling to both channels is taken to be equal, $J_i \equiv J$. In all calculations $J = 0.2$, and the Kondo temperature is $T_K = 1.16 \times 10^{-5}$. We use Wilson’s definition of the Kondo temperature⁶⁶ throughout this work.

It must be emphasized that even in the limit of small exchange couplings J_i , that is, when the Kondo effect plays no role and the impurity remains unscreened, the system still is not equivalent to a classical spin. The ground state for small J_i is a degenerate spin S multiplet, which is not equivalent to a single spin-polarized state as predicted by a classical spin model (the symmetries of the state are different). Another important observation is that, quite generally, in quantum impurity models one needs $\Delta \sim T_K$ to observe sub-gap excitations well inside the gap (i.e., not at the very edge), as shown in Table I. Thus in the situations where the spin-flip scattering processes play no role, we also do not expect to observe any sub-gap peaks deep in the gap. This is in contradiction to the results of the classical spin models, which on the one hand presume the irrelevance of the Kondo effect due to small exchange coupling, yet also predict excitations well inside the gap. Such a discrepancy exists even for the relatively large spin $S_{\text{imp}} = 5/2$, which still cannot be considered as a classical spin.

IV. TRANSITIONS IN THE ANISOTROPIC CASE

In the anisotropic case, the ground-state multiplet with $S \geq 1$ splits: for axial $D < 0$ anisotropy the new ground state consists of states with the maximal $S_z = \pm S$, while for planar $D > 0$ anisotropy the ground state is $S_z = 0$ for integer S and $S_z = \pm 1/2$ for half-integer S . The transition point at Δ_c in the isotropic models is extended into transition lines in the (D, Δ) plane. For a given value of D , there is some gap Δ where the system makes a transition from a “low- $|S_z|$ ” to a “high- $|S_z|$ ” regime, which are the equivalents of the Kondo-screened and free-spin regime, respectively. The

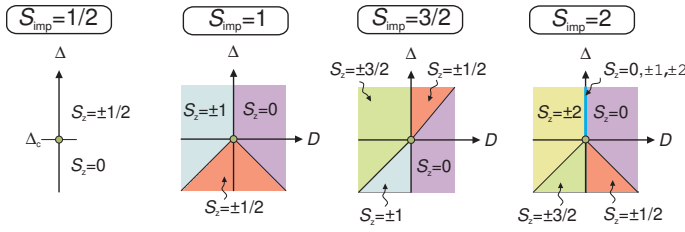


Figure 2: (Color online) Many-body ground state as a function of the gap Δ and the magnetic anisotropy D at fixed exchange coupling J for a range of the impurity spin S_{imp} in the single-channel case. Magnetic field is zero, $B = 0$. The value Δ_c (circle) corresponds to the transition point between the Kondo screened and unscreened impurity moment in the isotropic case.

results of extensive calculations for the single-channel problems are summarized in Fig. 2 in the form of phase diagrams, while the actual numerical results (including also all sub-gap excited states) are shown in the Appendix.

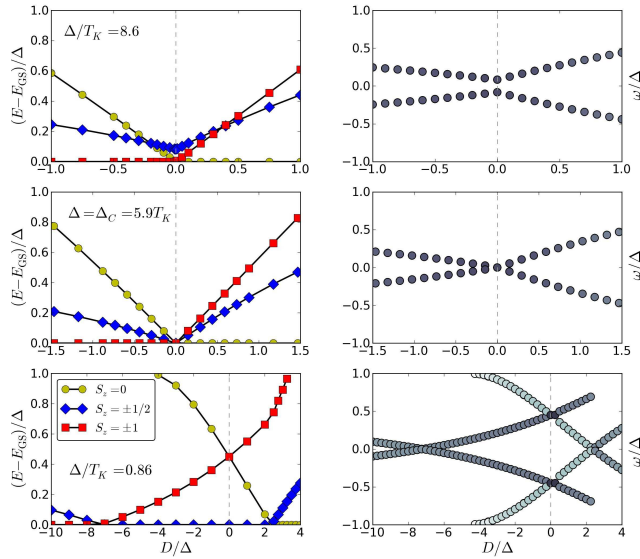


Figure 3: (Color online) Left panels: Ground state and sub-gap many-body excited states as a function of the magnetic anisotropy D for different values of the superconducting gap Δ for the single-channel spin-1 Kondo models. Zero magnetic field, $B = 0$. Top to bottom: “free-spin” regime, transition regime, Kondo screened regime. The energies E are plotted relative to the ground-state energy E_{GS} and they are rescaled in units of the gap, thus the ground state always lies atop the horizontal axis at $E = E_{\text{GS}}$ and the continuum of excitations starts at $(E - E_{\text{GS}})/\Delta = 1$. Right panels: Energies and weights of the sub-gap spectral peaks in the impurity spectral function. Darker shade corresponds to higher spectral weight of the delta peak.

Let us consider the results for $S_{\text{imp}} = 1$ more closely. In the left panels in Fig. 3 we plot the ground state as well as the sub-gap excited-state energies as a function of the anisotropy parameter D for three values of Δ that correspond in the

isotropic limit to the Kondo regime, the transition regime, and the “free-spin” regime, respectively. The spin-1 ground state and excited state (ES) spin multiplets split in the presence of the magnetic anisotropy. The degree of splitting is not the same as for free multiplets, but rather depends on Δ and T_K . For example, at $\Delta/T_K = 8.6$ we find

$$\begin{aligned} d(E_{S_z=1} - E_{S_z=0})/dD &= \langle 1|S_{\text{imp},z}^2|1\rangle - \langle 0|S_{\text{imp},z}^2|0\rangle \\ &\approx 0.867 - 0.266 \approx 0.6, \end{aligned} \quad (2)$$

rather than the free-impurity result 1. The anisotropy effects are thus significantly renormalized by the exchange coupling of the impurity with the host. This observation is important for the interpretation of possible experimental results: from the sub-gap excitation spectra, one cannot directly obtain the “bare” anisotropy parameters that appear in the Hamiltonian, only their effective “renormalized” values.

The transitions between the ground state and the excited states correspond to discrete (delta) sub-gap peaks in the differential conductance spectra. We plot the spectra of these peaks in the right panels of Fig. 3. Only the transitions between the ground state and the excited states with $\Delta S_z = \pm 1/2$ are observable spectroscopically. Multiple sub-gap peaks may be observed, for example, in the “Kondo regime” with $S_z = \pm 1/2$ ground state for $D \neq 0$. A characteristic feature is that some sub-gap peaks may disappear abruptly as a function of D/Δ when the ground state changes. We also note that in an interacting superconducting system, it is crucial to distinguish between the many-particle states (ground state and excited states) and the peaks in the spectral functions associated with transition between said states. Namely, to each many-particle excitation with energy E , such that $\Delta S_z = \pm 1/2$ with respect to the ground state, corresponds not one but two spectral peaks in the single-particle spectral function. They are located symmetrically at $\omega = \pm(E - E_{\text{GS}})$; it is possible, for example, to end up in exactly the same many-particle state by either adding an electron ($\omega > 0$ peak) or removing it ($\omega < 0$ peak). The lack of the distinction between the many-particle states and the spectral peaks has led to some confusion in the literature. The difference is particularly important for interacting systems, where the many-particle states cannot always be decomposed into products of single-particle levels (quasiparticles). A notable example is the two-channel $S_{\text{imp}} = 1/2$ model.

In fully general multi-channel problems with non-equal J_i , there are multiple stages of the Kondo screening with different Kondo temperatures, $T_K^{(i)}$, $i = 1, \dots, N$. Depending on the relation between Δ and all $T_K^{(i)}$, the system may end up in different ground states. As an illustration, in Fig. 4 we depict the possible ground states for isotropic $N = 2$ problems by fixing Δ and plotting the phase diagrams in the (J_1, J_2) plane. The case of $S_{\text{imp}} = 1/2$ is special due to the overscreening effects. The second case with $S_{\text{imp}} = 1$ shows the generic phase diagram for all $S_{\text{imp}} \geq 1$ and $N = 2$: in the vicinity of the equal-coupling line, the ground-state spin changes by $N/2 = 1$, while for general J_i the multiple Kondo scales $T_K^{(i)}$ result in intermediate regimes with only partial impurity screening. This is a new feature that is particular to multi-

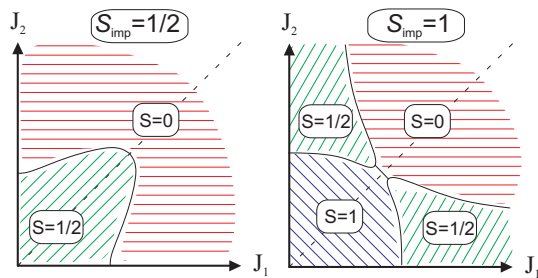


Figure 4: (Color online) Schematic diagram representing the many-body ground state as a function of the exchange coupling constants J_1 and J_2 for the isotropic ($D = 0$) two-channel $S_{\text{imp}} = 1/2$ and $S_{\text{imp}} = 1$ Kondo models at fixed superconducting gap $\Delta = 10^{-5}$. Zero magnetic field, $B = 0$.

channel problems. In the presence of anisotropy D , the phase diagrams in Fig. 4 may be extended into the third dimension; the GS multiplets with $S \geq 1$ split according to the sign of D , and effects similar to those represented in Fig. 2 are observed. (See Fig. 16 for some results of the calculations at finite magnetic anisotropy D .)

V. SUB-GAP EXCITED STATES AND SPECTRAL PEAKS IN THE MULTI-CHANNEL CASE

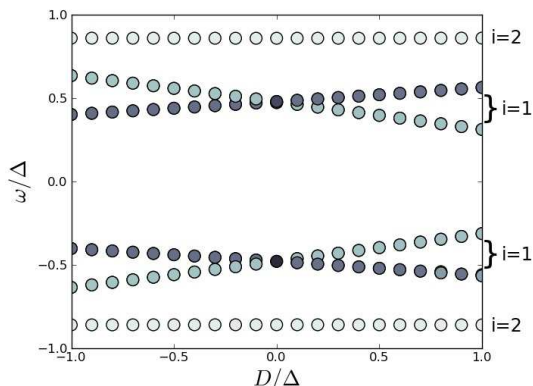


Figure 5: Energies and weights of the sub-gap peaks for the two-channel $S_{\text{imp}} = 1$ Kondo model as a function of the magnetic anisotropy. Parameters are $\Delta = 10^{-5}$, $J_1 = 0.2$, and $J_2 = 0.1$. Darker shade corresponds to higher spectral weight. The labels $i = 1$ and $i = 2$ indicate spectral peaks associated with the i -th scattering channel. Zero magnetic field, $B = 0$.

For real transition-metal impurities on a surface, the exchange coupling constants depend on the energies and the hybridization constants of the d orbitals. Assuming an adsorption site of low symmetry, it is generally more likely that one of the exchange constants, say J_1 , will be dominant. In strict single-channel problems, there is always at least one excited state inside the gap. It tends to be located at the gap edge for $T_K \ll \Delta$ and $T_K \gg \Delta$, but it is found well inside the gap when T_K and Δ are roughly of the same order of magnitude.

In the presence of additional scattering channels, further sub-gap excitations may appear. For $N = 2$, we find, however, that if J_2 is much lower than J_1 , the additional excited state merges with the continuum and is not observable. For moderate J_2/J_1 ratio, the channel-2 excitation peak is still inside the gap, but its spectral weight tends to be much smaller than that in the dominant $i = 1$ channel.

On more symmetric surfaces (adsorption sites), some of the exchange coupling constants J_i can be equal, for example pair-wise equal in the presence of a four-fold symmetry axis. In this case, the excitations associated with those J_i that are equal will be degenerate, thus multiple sub-gap peaks are again not expected.

These results suggest that it is not very likely to observe multiple peaks due to coupling to different scattering channels. Given that multiple peaks are nonetheless commonly observed in experiments¹⁹⁻²¹, we propose that a very likely interpretation involves the presence of the magnetic anisotropy splitting of the sub-gap excitations. An example for $N = 2$ is shown in Fig. 5. For $D = 0$, the ground state is $S = 1/2$ and there is an $S = 1$ excited state associated with channel 1 and an $S = 0$ excited state associated with channel 2. For $D \neq 0$, the triplet excited state splits. In the presence of longitudinal anisotropy, the peaks will split at most in two, but additional splitting may be induced by the transverse anisotropy $E(S_x^2 - S_y^2)$, which is also known to be present in adsorbed magnetic impurities²⁵.

VI. BEHAVIOR IN THE EXTERNAL MAGNETIC FIELD

Due to the strongly enhanced spin-orbit interaction on surfaces, the interpretation of multiple peaks in terms of magnetic anisotropy splitting appears very plausible. To experimentally distinguish between the different possible origins of the multiple-peak sub-gap structures in a conclusive way, we propose to study the Zeeman splitting of the sub-gap peaks by weak magnetic fields (weak enough so that the superconductivity is not significantly suppressed; see also Refs. 82-85). This is possible because magnetic atoms adsorbed on the surface of a superconductor are not fully shielded by the Meissner effect. Ultra-low-temperature STM's equipped with dilution refrigerators are likely to achieve sufficient energy resolution. The magnetic field splits pairs of the sub-gap states with the same $|S_z|$. Since the only observable transitions are those with $\Delta S_z = \pm 1/2$, each spectral peak may split at most in two. In the presence of transverse anisotropy and/or transverse magnetic field, the spin symmetry is fully lifted and even more complex spectra of excitation peaks can arise. We note, however, that if the ground state is spin degenerate (i.e., for partially screened impurity), even a small magnetic field can fully polarize the residual impurity spin, thus some of the sub-gap peaks might not be spectroscopically observable since their weights are essentially zero (at $T = 0$). Some observed peaks will thus merely shift, rather than split. This behavior is represented schematically in Fig. 6 for the example of an $S_{\text{imp}} = 1/2$ impurity in the single-channel case, while the results of a corresponding NRG calculation are shown in

Fig. 7(a).

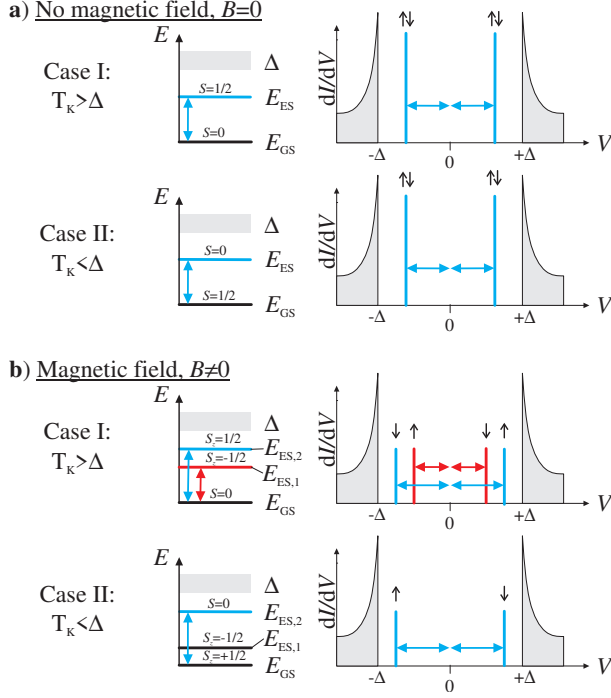


Figure 6: (Color online) Schematic representation of the relation between the many-body energy levels (shown on the left; E_{GS} is the ground-state energy, E_{ES} are the excited-state energies, Δ is the gap beyond which starts the continuum of the conduction-band states) and the spectral peaks which can be measured by the STM (shown on the right; $V > 0$ indicates tunneling into “empty” states, i.e., the electron addition transitions, while $V < 0$ corresponds to the removal of electrons from the system). Only transitions where S_z changes by $1/2$ are spectroscopically visible at very low temperatures. The arrows indicate the spin of the electron being added (positive V) or removed (negative V) from the system at the given resonance. In the absence of the field, $T_K > \Delta$ and $T_K < \Delta$ cases cannot be easily distinguished spectroscopically since they both exhibit a pair of excitation peaks at $\omega = \pm(E_{ES} - E_{GS})$. In the magnetic field, we expect to observe peak splitting for $T_K > \Delta$, and while for $T_K < \Delta$ we expect merely a shift of the peak pair concomitant with the weight reduction if the experimental temperature is much lower than the $E_{ES,1} - E_{GS}$ scale. The example depicted in the plot corresponds to an $S_{imp} = 1/2$ magnetic impurity in the single-channel case.

The single-channel $S_{imp} = 1$ model is studied in Fig. 7b,c,d) for different values of the magnetic anisotropy D . In the absence of the anisotropy, $D = 0$, the behavior is similar to that in the spin- $1/2$ case: for $\Delta/T_K > 0$ (“free-spin” regime), the peaks merely shift, while for $\Delta/T_K < 0$ (Kondo regime), there is a splitting of the peaks, since the transitions are possible from the low-lying doublet state (here $S_z = -1/2$) to both $S_z = -1$ and $S_z = 0$ excited states. It is worth emphasizing that in the latter case, the peak weights are different for the two transitions. A simplified, but intuitive picture is the following: the ground state is a Kondo state $|S_{imp,z} = -1, \uparrow\rangle$, that is, a bound state of an $S_z = -1$ impurity state and a spin-up conduction-band electron with total

$S_z = -1/2$. The first excited state has $S_z = -1$ and can be obtained in the process of adding a spin-down electron. The second excited state has $S_z = 0$ and it can be reached by adding a spin-up electron. Since there is already a spin-up electron present in the Kondo ground state, adding a further spin-up electron will have a reduced weight as compared to adding a spin-down electron. This behavior persists in the presence of magnetic anisotropy: the peak corresponding to a transition to the $S_z = 0$ state has lower weight than the peak corresponding to the transition to the $S_z = -1$ state in all three cases of $D = 0$, $D > 0$, and $D < 0$; see Fig. 7b,c,d).

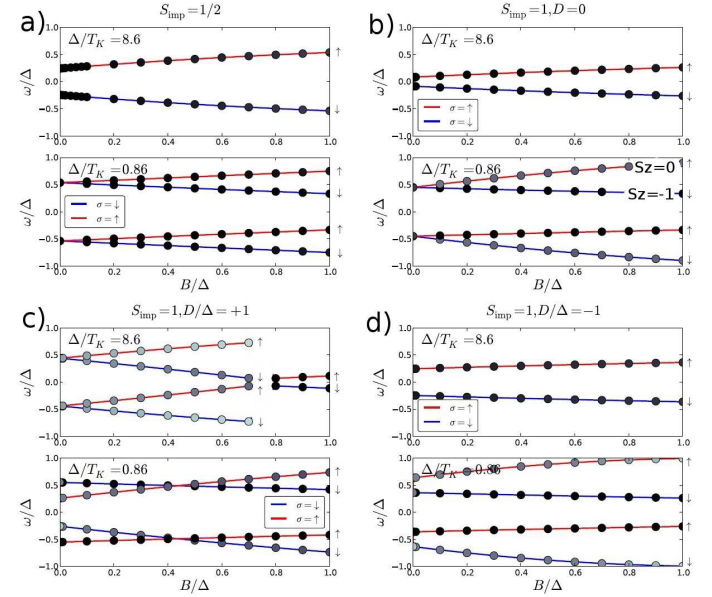


Figure 7: (Color online) Energies and weights of the sub-gap spectral peaks as a function of the external magnetic field for the single-channel spin- $1/2$ and spin- 1 Kondo models with different magnetic anisotropy terms.

In the “free-spin” regime, the evolution of the spectral peaks in the magnetic field depends on the sign of the magnetic anisotropy; compare the upper panels in Fig. 7b,c,d). The isotropic $D = 0$ and easy-axis $D < 0$ cases are similar: in the presence of the field, the $S_z = -1$ state will be the ground state and the transitions are only possible to the $S_z = -1/2$ excited state, thus a single sub-gap peak pair is observed. The easy-plane $D > 0$ case is more interesting. Now the ground state (for small magnetic fields) is $S_z = 0$, thus the transitions to both $S_z = +1/2$ and $S_z = -1/2$ excited states are possible; we thus see two pairs of sub-gap spectral peaks, that is, a total of four sharp peaks. For very large Zeeman splitting, the $S_z = -1/2$ excited state will become the new ground state of the system; at this point only the transition to the $S_z = 0$ sub-gap will be possible and a single pair of peaks will remain in the impurity spectral function.

In Fig. 8, we finally plot the field dependence of the spectral peaks of a two-channel spin- 1 impurity for different magnetic anisotropies D . In all three cases, the ground state for $B > 0$ is non-degenerate, $S_z = -1/2$, and one may only observe the transitions to $S_z = -1$ and $S_z = 0$ excited states. As

evidenced by the results in Fig. 8, the sign and magnitude of D can be easily determined from the shifts. The peak due to the second weakly coupled conduction channel is always weaker as compared to the peaks associated with the dominant screening channel.

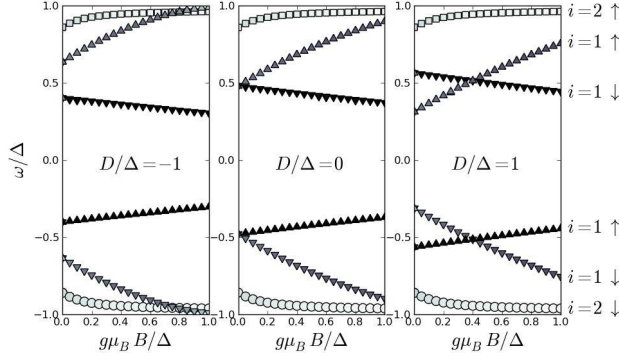


Figure 8: Energies and weights of the sub-gap spectral peaks as a function of the magnetic field B for the two-channel $S_{\text{imp}} = 1$ impurity. Parameters are as in Fig. 5. The spectral peaks are fully spin-polarized, as indicated by the arrows.

VII. EFFECTS OF THE INTER-IMPURITY EXCHANGE INTERACTION

When adsorbed magnetic impurities are brought together, for example by controlled manipulation using the tip of the STM, their mutual interaction will change the LDOS signatures measured by the scanning tunneling spectroscopy^{19,86-90}. The theory of the inter-impurity interactions in the normal case has been worked out using both simplified model Hamiltonians and ab initio calculations⁹¹⁻⁹⁵. In the superconducting case, the calculations of the sub-gap excitation spectra in impurity dimers have been performed mainly for classical impurity spins^{96,97}. Recently, some calculations for coupled quantum impurities have been performed in the context of double quantum dots⁹⁸. Here we study the problem of two quantum impurities, each coupled to a separate conduction band with a superconducting gap (with equal Δ), and interacting via an isotropic Heisenberg Hamiltonian:

$$H_{\text{int}} = JS_{\text{imp},1} \cdot S_{\text{imp},2}. \quad (3)$$

We first discuss the simplest case of two $S_{\text{imp}} = 1/2$ impurities. The numerical results for the sub-gap states are shown in Fig. 9. The parameters are chosen such that in the absence of coupling, each impurity is the Kondo screened regime with an $S = 0$ ground state and one $S = 1/2$ sub-gap excited state (two-fold degenerate due to spin); for the two-impurity system, the ground state is thus a singlet (we will call it the “Kondo singlet”), and there are two degenerate $S = 1/2$ excited states (four-fold total degeneracy). As the antiferromagnetic ($J > 0$) exchange coupling is turned on, a new singlet state emerges from the continuum; this state can be interpreted

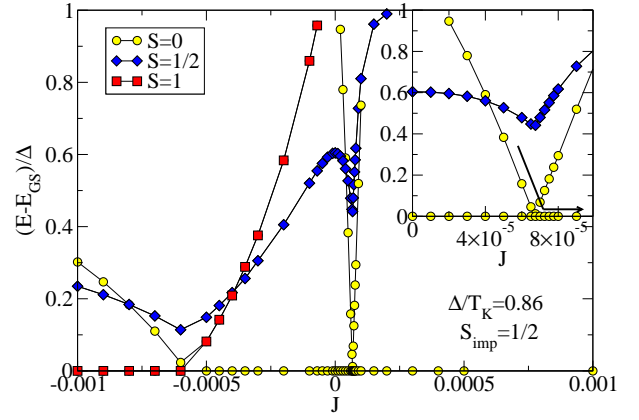


Figure 9: (Color online) Ground state and sub-gap many-body excited states in the two-impurity problem with $S_{\text{imp}} = 1/2$ impurities coupled by Heisenberg exchange coupling J . The inset is a close-up view of the region where the two different singlet ground states cross: the arrow shows the evolution of the local AFM-ordered spin-singlet ground state as J is increased. The gap is $\Delta = 10^{-5}$.

as arising from the antiferromagnetically ordered local singlet state formed by the two impurity spins, and we will therefore denote it as the “AFM singlet”. It should be emphasized that this state is not directly related to the $S = 1/2$ excited states (which are actually present in the sub-gap spectrum at the same time as the new AFM singlet); the AFM singlet state should thus not be interpreted as emerging from the coupling of the $S = 1/2$ sub-gap localized states, but rather as arising from the local inter-impurity singlet state. We furthermore emphasize that the two $S = 1/2$ excited states remain degenerate (this holds, in fact, for all values of J). As J is increased beyond $J \approx 6 \times 10^{-5}$, the Kondo and AFM singlet states cross and exchange their roles as the ground and the excited state. At still higher J , both the excited Kondo singlet state and the two $S = 1/2$ excited states merge with the continuum and are no longer observable. For large antiferromagnetic inter-impurity coupling, the dimer behaves as a non-magnetic object and therefore does not have any excitations deep inside the gap. Such behavior seems to be present for Cr dimers (in the configuration “Cr dimer II” with small inter-atom separation)¹⁹.

Equally interesting is the case of ferromagnetic Heisenberg coupling, also shown in Fig. 9. In this case, a new “FM triplet” sub-gap state emerges in the sub-gap spectrum. This state decreases in energy until it replaces the Kondo singlet as the new ground state. Two important observations can be made: (i) the level crossing between the FM triplet and the Kondo singlet occurs for a much larger (by an order of magnitude) absolute value of the Heisenberg coupling as the level crossing between the AFM singlet and the Kondo singlet; (ii) with increasing $|J|$, the Kondo singlet and the degenerate $S = 1/2$ excited states evolve only slowly and remain deep inside the gap even for very large ferromagnetic exchange coupling. This suggests that in the case of ferromagnetic dimers, we are more likely to observe some sub-gap spectral peaks. It is possible that the Mn dimers (even in the configuration “Mn dimer II”

with small inter-atom separation¹⁹) have ferromagnetic spin coupling.

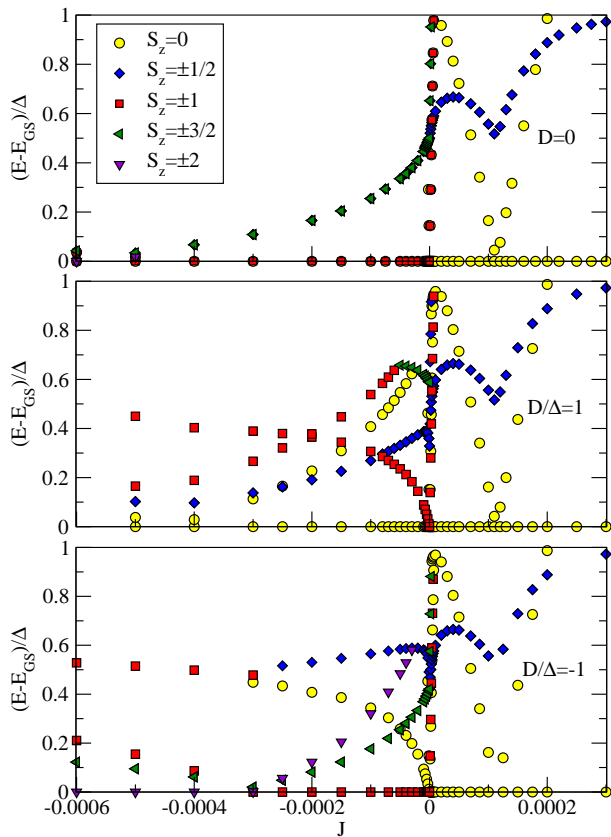


Figure 10: (Color online) Ground state and sub-gap many-body excited states in the two-impurity problem with $S_{\text{imp}} = 1$ impurities coupled by Heisenberg exchange coupling J . The gap is $\Delta = 10^{-5}$.

We now turn to the case of two isotropic $S_{\text{imp}} = 1$ impurities, each coupled to a single channel; see the upper panel in Fig. 10. We again consider the parameter regime where each impurity is Kondo-screened. This time, however, the impurities have residual spin 1/2. In the absence of the inter-impurity coupling, the ground state is degenerate and composed of a singlet and a triplet “Kondo state”, and there are degenerate excited states with $S = 1/2$ and $S = 3/2$. The ground-state degeneracy is lifted by a small J , thus for small J the ground state is either a singlet (for $J > 0$) or a triplet (for $J < 0$); this splitting occurs on the energy scale of almost “bare” J ; see the close-up view in Fig. 11. For antiferromagnetic exchange coupling, there is an additional singlet state that arises from the local inter-impurity singlet state in which two $S = 1$ spins are rigidly antiferromagnetically ordered. This state is different from the singlet Kondo state, which arises from AFM ordering between two residual $S = 1/2$ extended objects. This is another confirmation of the nature of the sub-gap singlet states, which we had already discussed in the case of $S_{\text{imp}} = 1/2$. For sufficiently large AFM coupling, the singlet states cross, and for very large coupling we again find that there are no sub-gap excited states. Note also the similarity between the $J > 0$ behavior in $S_{\text{imp}} = 1/2$ and

$S_{\text{imp}} = 1$ models.

For ferromagnetic coupling, the situation is again similar to what we had observed for $S_{\text{imp}} = 1/2$ impurities: the ferromagnetically ordered $S = 2$ local object becomes the new ground state only for very large Heisenberg coupling. The transition occurs at $J \approx -6 \times 10^{-5}$, that is, at essentially the same value as for $S_{\text{imp}} = 1/2$. In addition, we again observe that some sub-gap excited states are typically found in the sub-gap spectrum even for large $|J|$.

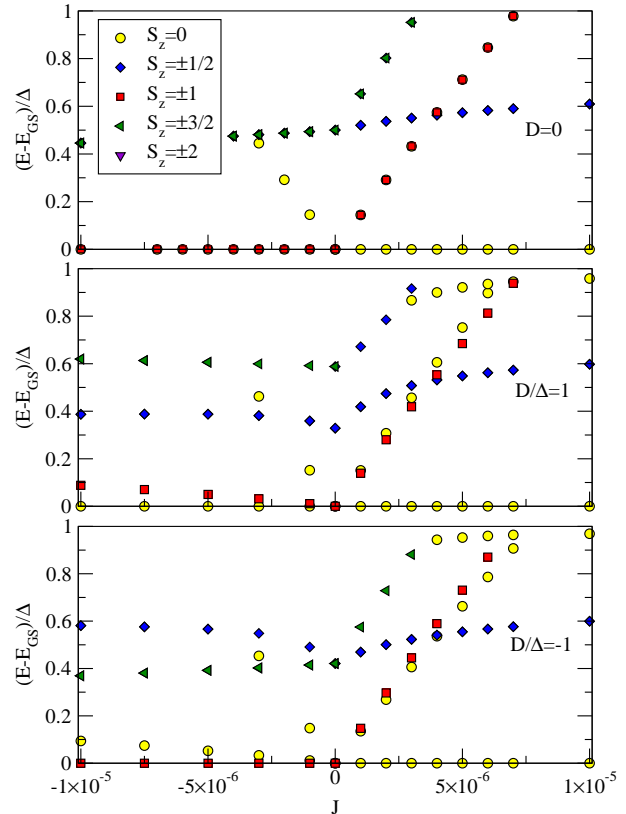


Figure 11: (Color online) Close-up view of the small- J region in Fig. 10.

Finally, we discuss how the sub-gap excitation spectra change in the presence of the magnetic anisotropy. In the two lower panels in Fig. 10, we show the results for easy-plane and easy-axis magnetic anisotropy for the $S_{\text{imp}} = 1$ impurities. The results are in general similar to those for the isotropic model, but there are some notable differences.

For AFM coupling, we find that the ground state is an $S_z = 0$ state (i.e., the “singlet” state) and that there are no sub-gap excited states for large enough J . In fact, it may be noticed that the results for $J > 0$ are remarkably similar irrespective of the sign and strength of the magnetic anisotropy.

For small ferromagnetic exchange coupling, the $S = 1$ ground state splits: for easy-plane anisotropy the ground state is $S_z = 0$, while for easy-axis anisotropy it is $S_z = \pm 1$. Thus the combined inter-impurity states can be understood within a two-stage splitting model: in the first step, we consider how the states combine due to the Heisenberg exchange coupling; in the second step, we consider how the resulting

states split due to the magnetic anisotropy. Such separation is possible because in the parameter regime under consideration, the scale of the exchange splitting (up to several times 10^{-4}) is larger than the scale of the magnetic anisotropy (fixed at $|D| = 10^{-5}$). For strong FM coupling, the result depends on the type of anisotropy: the ground state arises from an $S = 2$ state, but for the easy-plane case the actual ground state is a non-degenerate $S_z = 0$ state, while for the easy-axis case the ground state is a twofold-degenerate $S_z = \pm 2$ state. The transition between the small- $|J|$ and large- $|J|$ ground state occurs at a value of J that depends on the magnetic anisotropy.

VIII. CONCLUSION

We have studied single magnetic impurities on superconductor surfaces as well as their dimers. We have emphasized the importance of using quantum impurity models to describe the sub-gap excitation spectrum of the magnetic adatoms. The isotropic models exhibit a transition between ground states with different degrees of Kondo screening of the impurity spin; this depends on the values of the Kondo exchange coupling constants and the ratios between the resulting Kondo temperatures and the BCS superconducting gap. The sub-gap excited states only appear in cases where at least one of the Kondo temperature scales is of the same order as the superconducting gap. If all coupling constants are small (i.e., if the Kondo effect is absent), there are no sub-gap excited states deep inside the gap, which is at odds with the predictions from the classical spin models. The ground state and sub-gap excited states with $S \geq 1$ are split in the presence of the magnetic anisotropy. It is found that the splitting is strongly renormalized by the Kondo screening, thus the model needs to be studied using non-perturbative techniques, such as the numerical renormalization group. We find that the weight of the sub-gap peaks is the largest for strongly coupled Kondo channels, but becomes lower for weakly coupled channels. In addition, the sub-gap excitations associated with weakly coupled channels tend to appear near the gap edge, and may

therefore be difficult to observe. This finding suggests that multiple-peak sub-gap excitations likely arise from the internal structure of the impurity (spin-orbit coupling leading to the magnetic anisotropy). We have also explored the interdot exchange coupling for impurity dimers: for strong antiferromagnetic coupling, no sub-gap excitations are present, while even for relatively strong ferromagnetic coupling some sub-gap peaks may be observable. We have shown that the external magnetic field has a sizable effect on the sub-gap excitation spectra of impurities. Exploring the magnetic properties of impurities using the field dependence of the sub-gap peaks constitutes a worthwhile experimental challenge. Furthermore, using a break-junction setup with superconducting contacts should make it possible to map the excitation spectra in the entire (D, B) plane at the same time, providing further means to test the predictions of this work.

Acknowledgments

RZ would like to thank E. Tosatti and M. Fabrizio for interesting discussions. R.Z. acknowledges the support of the Slovenian Research Agency (ARRS) under Grant No. Z1-2058. T.P. acknowledges support by the Deutsche Forschungsgemeinschaft through SFB 602.

Appendix A: Sub-gap excitation spectra

This appendix contains additional figures detailing the results discussed in the main text. Figures 12 and 13 show the sub-gap states for one-channel and two-channel Kondo models from which the transition points between the (partially) screened and unscreened regimes can be extracted; see Table I and Figure 2 in the main text. Fig. 14 shows the effect of the magnetic anisotropy on the sub-gap states, that is, the splitting of the degenerate spin multiplets. Figures 15 and 16 contain the results for the two-channel $S = 1/2$ and $S = 1$ Kondo model in the (J_1, J_2) plane, which serve to establish the phase diagram in Fig. 4.

-
- ¹ I. Giaever, Phys. Rev. Lett. **5**, 147 (1960).
² I. Giaever, Rev. Mod. Phys. **46**, 245 (1974).
³ S. H. Pan, E. W. Hudson, K. M. Lang, H. Eisaki, S. Uchida, and J. C. Davis, Nature **403**, 746 (2000).
⁴ A. Yazdani, C. M. Howald, C. P. Lutz, A. Kapitulnik, and D. M. Eigler, Phys. Rev. Lett. **83**, 176 (1999).
⁵ A. V. Balatsky, I. Vekhter, and J.-X. Zhu, Rev. Mod. Phys. **78**, 373 (2006).
⁶ O. Fischer, M. Kugler, I. Maggio-Aprile, and C. Berthod, Rev. Mod. Phys. **79**, 353 (2007).
⁷ G. Binnig, H. Rohrer, C. Gerber, and E. Weibel, Phys. Rev. Lett. **49**, 57 (1982).
⁸ N. D. Lang, Phys. Rev. B **34**, 5947 (1986).
⁹ M. F. Crommie, C. P. Lutz, and D. M. Eigler, Phys. Rev. B **48**, 2851 (1993).
¹⁰ A. Yazdani, B. A. Jones, C. P. Lutz, M. F. Crommie, and D. M. Eigler, Science **275**, 1767 (1997).
¹¹ D. J. Derro, E. W. Hudson, K. M. Lang, S. H. Pan, J. C. Davis, J. T. Markert, and A. L. de Lozanne, Phys. Rev. Lett. **88**, 097002 (2002).
¹² A. J. Heinrich, J. A. Gupta, C. P. Lutz, and D. M. Eigler, Science **306**, 466 (2004).
¹³ J. A. Stroscio and R. J. Celotta, Science **306**, 242 (2004).
¹⁴ N. Néel, J. Kröger, L. Limot, K. Palotas, W. A. Hofer, and R. Berndt, Phys. Rev. Lett. **98**, 016801 (2007).
¹⁵ Y. Yayon, V. W. Brar, L. Senapati, S. C. Erwin, and M. F. Crommie, Phys. Rev. Lett. **99**, 067202 (2007).
¹⁶ H. Alloul, J. Bobroff, M. Gabay, and P. J. Hirschfeld, Rev. Mod. Phys. **81**, 45 (2009).
¹⁷ H. Brune and P. Gambardella, Surf. Sci. **602**, 1812 (2009).
¹⁸ M. Ternes, A. J. Heinrich, and W. D. Schneider, J. Phys.: Condens. Matter **21**, 053001 (2009).
¹⁹ S. H. Ji, T. Zhang, Y. S. Fu, X. Chen, X.-C. Ma, L. Li, W.-H. Duan, J.-F. Jia, and Q.-K. Xue, Phys. Rev. Lett. **100**, 226801 (2008).

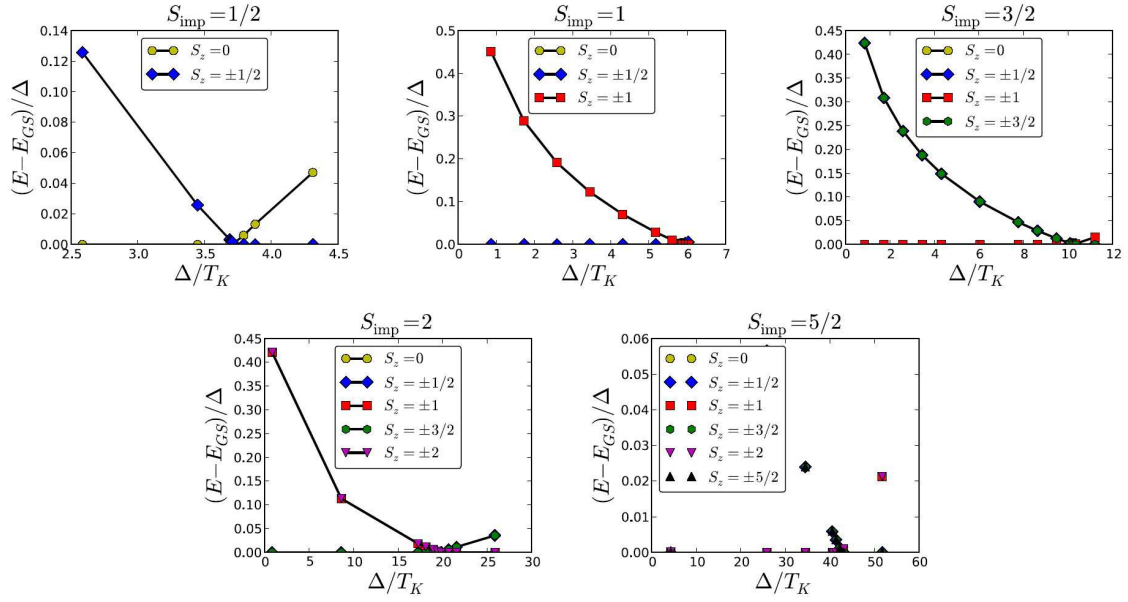


Figure 12: (Color online) Ground state and sub-gap many-body excited states as a function of the superconducting gap Δ for single-channel ($N = 1$) Kondo models with different impurity spin S_{imp} . The NRG calculations have been performed with the NRG discretization parameter $\Lambda = 2$. Additional Λ -scaling calculations suggest that the results for the transition point Δ_c/T_K given in Table 1 are accurate within few percent.

- ²⁰ M. Iavarone, G. Karapetrov, J. Fedor, D. Rosenmann, T. Nishizaki, and N. Kobayashi, *J. Phys.: Condens. Matter* **22**, 015501 (2010).
- ²¹ S.-H. Ji, T. Zhang, Y.-S. Fu, X. Chen, J.-F. Jia, Q.-K. Xue, and X.-C. Ma, *Appl. Phys. Lett.* **96**, 073113 (2010).
- ²² M. E. Flatté and J. M. Byers, *Phys. Rev. Lett.* **78**, 3761 (1997).
- ²³ M. E. Flatté and J. M. Byers, *Phys. Rev. B* **56**, 11213 (1997).
- ²⁴ P. Gambardella, S. Rusponi, M. Veronese, S. S. Dhesi, C. Grazioli, A. Dallmeyer, I. Cabria, R. Zeller, P. H. Dederichs, K. Kern, et al., *Science* **300**, 1130 (2003).
- ²⁵ C. F. Hirjibehedin, C.-Y. Lin, A. F. Otte, M. Ternes, C. P. Lutz, B. A. Jones, and A. J. Heinrich, *Science* **317**, 1199 (2007).
- ²⁶ J. J. Parks, A. R. Champagne, T. A. Costi, W. W. Shum, A. N. Papaty, E. Neuscamman, S. Flores-Torres, P. S. Cornaglia, A. A. Aligia, C. A. Balseiro, et al., *Science* **328**, 1370 (2010).
- ²⁷ H. Shiba, *Prog. Theor. Phys.* **40**, 435 (1968).
- ²⁸ A. Sakurai, *Prog. Theor. Phys.* **44**, 1472 (1970).
- ²⁹ J. Zittartz and E. Müller-Hartmann, *J. Physik* **232**, 11 (1970).
- ³⁰ J. E. Moore, *Nature* **464**, 194 (2010).
- ³¹ L. Fu, C. L. Kane, and E. J. Mele, *Phys. Rev. Lett.* **98**, 106803 (2007).
- ³² D. Hsieh, Y. Xia, L. Wray, D. Qian, A. Pal, J. H. Dil, J. Osterwalder, F. Meier, G. Bihlmayer, C. L. Kane, et al., *Science* **323**, 919 (2009).
- ³³ P. Roushan, J. Seo, C. V. Parker, Y. S. Hor, D. Hsieh, D. Qian, A. Richardella, M. Z. Hasan, R. J. Cava, and A. Yazdani, *Nature* **460**, 1106 (2009).
- ³⁴ L. Fu, *Phys. Rev. Lett.* **103**, 266801 (2009).
- ³⁵ Z. Alpichshev, J. G. Analytis, J.-H. Chu, I. Fisher, Y.L.Chen, Z. Shen, A. Fang, and A. Kapitulnik, *Phys. Rev. Lett.* **104**, 016401 (2010).
- ³⁶ T. Zhang, P. Cheng, X. Chen, J.-F. Jia, X. Ma, K. He, L. Wang, H. Zhang, X. Dai, Z. Fang, et al., *Phys. Rev. Lett.* **103**, 266803 (2009).
- ³⁷ H.-M. Guo and M. Franz, *Phys. Rev. B* **81**, 041102(R) (2010).
- ³⁸ Q. Liu, C.-X. Liu, C. Xu, X.-L. Qi, and S.-C. Zhang, *Phys. Rev. Lett.* **102**, 156603 (2009).
- ³⁹ X. Zhou, C. Fang, W.-F. Tsai, and J. Hu, *Phys. Rev. B* **80**, 245317 (2009).
- ⁴⁰ X.-Y. Feng, W.-Q. Chen, J.-H. Gao, Q.-H. Wang, and F.-C. Zhang, *Phys. Rev. B* **81**, 235411 (2010).
- ⁴¹ R. Žitko, *Phys. Rev. B* **81**, 241414(R) (2010).
- ⁴² J. J. Cha, J. R. Williams, D. Kong, S. Meister, H. Peng, A. J. Bestwick, P. Gallagher, D. Goldhaber-Gordon, and Y. Cui, *Nano Letters* **10**, 1076 (2010).
- ⁴³ K. Satori, H. Shiba, O. Sakai, and Y. Shimizu, *J. Phys. Soc. Japan* **61**, 3239 (1992).
- ⁴⁴ O. Sakai, Y. Shimizu, H. Shiba, and K. Satori, *J. Phys. Soc. Japan* **62**, 3181 (1993).
- ⁴⁵ T. Yoshioka and Y. Ohashi, *J. Phys. Soc. Japan* **67**, 1332 (1998).
- ⁴⁶ T. Yoshioka and Y. Ohashi, *J. Phys. Soc. Japan* **69**, 1812 (2000).
- ⁴⁷ A. F. Otte, M. Ternes, K. von Bergmann, S. Loth, H. Brune, C. P. Lutz, C. F. Hirjibehedin, and A. J. Heinrich, *Nature Physics* **4**, 847 (2008).
- ⁴⁸ M. Lee, T. Jonckheere, and T. Martin, *Phys. Rev. Lett.* **101**, 146804 (2008).
- ⁴⁹ M. Lee, T. Jonckheere, and T. Martin, *Phys. Rev. B* **81**, 155114 (2010).
- ⁵⁰ M. Koga and M. Matsumoto, *Phys. Rev. B* **65**, 094434 (2002).
- ⁵¹ M. Matsumoto, M. Koga, and H. Kusunose, *J. Phys. Soc. Japan* **78**, 084718 (2009).
- ⁵² C. P. Moca, E. Demler, B. Jankó, and G. Zaránd, *Phys. Rev. B* **77**, 174516 (2008).
- ⁵³ R. Žitko, R. Peters, and T. Pruschke, *Phys. Rev. B* **78**, 224404 (2008).
- ⁵⁴ R. Žitko, R. Peters, and T. Pruschke, *New J. Phys.* **11**, 053003 (2009).
- ⁵⁵ C. Romeike, M. R. Wegewijs, W. Hofstetter, and H. Schoeller, *Phys. Rev. Lett.* **96**, 196601 (2006).
- ⁵⁶ M. N. Leuenberger and E. R. Mucciolo, *Phys. Rev. Lett.* **97**,

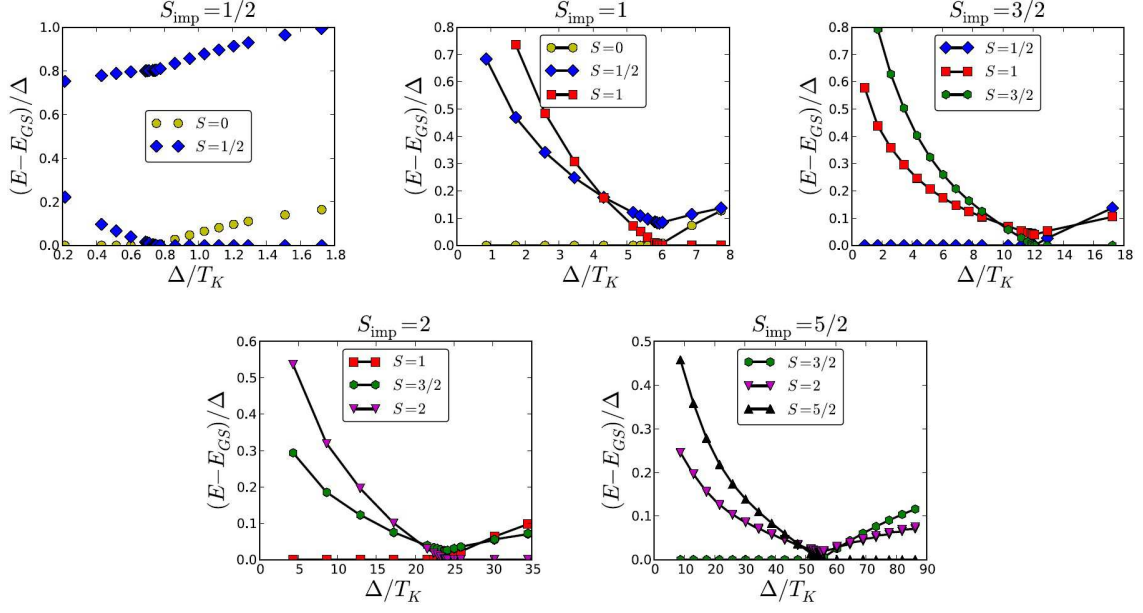


Figure 13: (Color online) Ground-state and sub-gap many-body excited states as a function of the superconducting gap Δ for two-channel ($N = 2$) Kondo models with different impurity spin S_{imp} . The NRG calculations have been performed with the discretization parameter $\Lambda = 4$. The results given in Table 1 for the two-channel case have been calculated by performing further calculations using a twist parameter $z = 0.5$ and averaging the results for $z = 1$ and $z = 0.5$. The tabulated results are then accurate within a few percent for both the single-channel and the two-channel case. Note the presence of the additional $S = S_{\text{imp}} - 1/2$ excited-state multiplet inside the gap. For non-equal J_i , this excited state can become the ground state in some parameter regimes; see Fig. 4.

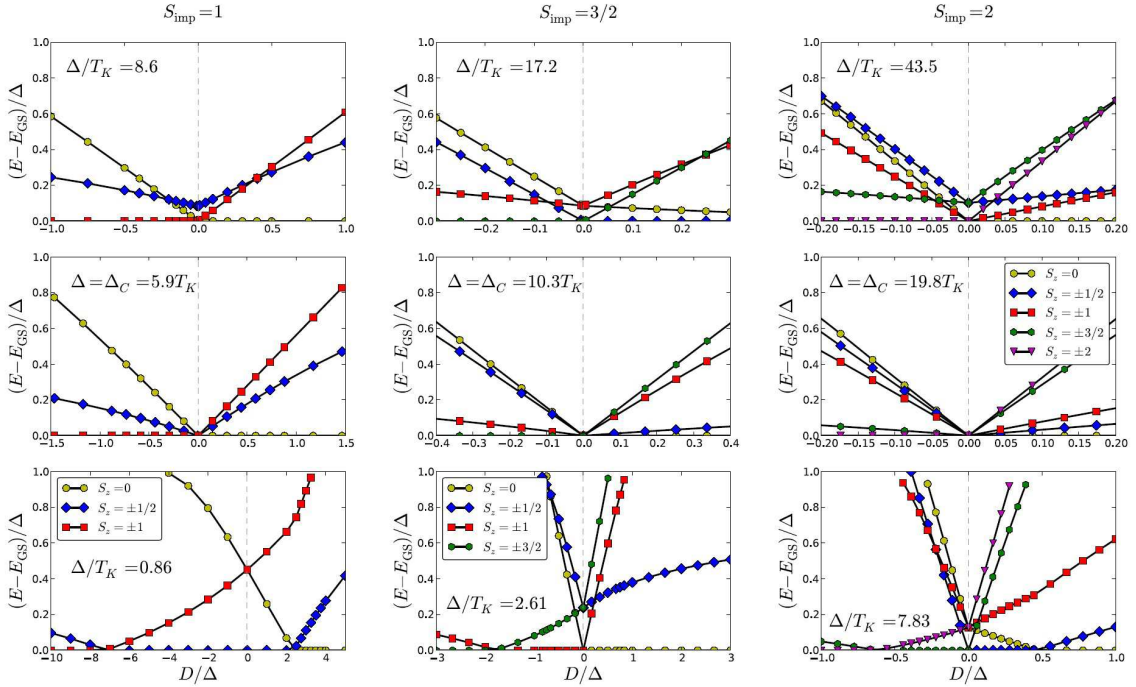


Figure 14: (Color online) Ground-state and sub-gap excited states as a function of the magnetic anisotropy D for different values of the superconducting gap Δ for the single-channel spin-1, spin-3/2, and spin-2 Kondo models. The results of these (and similar) calculations have been used to establish the schematic phase diagrams shown in Fig. 2.

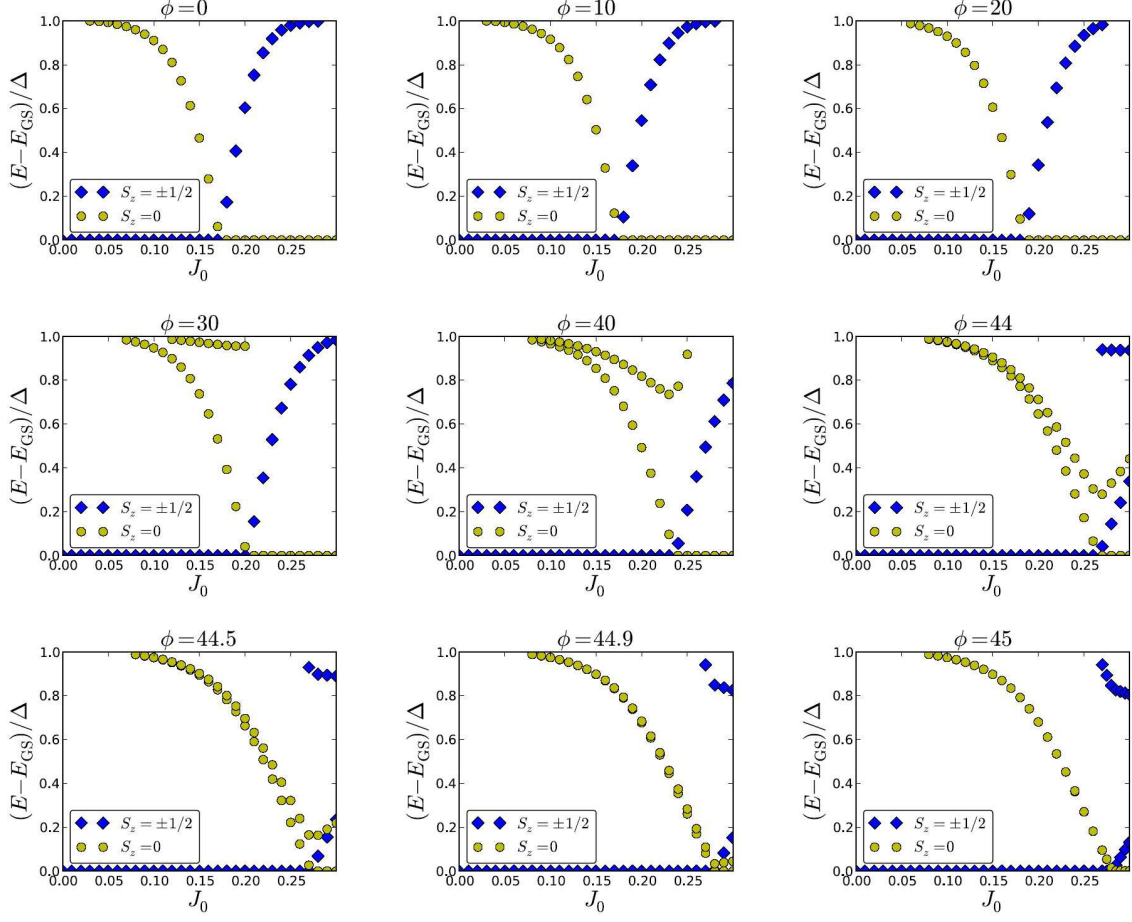


Figure 15: (Color online) Ground state and sub-gap excitations as a function of the parameter J_0 for the two-channel $S_{\text{imp}} = 1/2$ Kondo model. We define $J_1 = J_0 \cos \phi$ and $J_2 = J_0 \sin \phi$; the angles ϕ of the direction in the (J_1, J_2) plane are given (in degrees) as the titles of the subfigures. The gap is $\Delta = 10^{-5}$. The results of these (and similar) calculations have been used to establish the schematic phase diagram for the $S_{\text{imp}} = 1/2$ case in Fig. 4 of the main text. The two-channel calculations with non-equal J_i have to be performed with a higher value of the NRG discretization parameter $\Lambda = 8$, otherwise they are intractable. No twist-parameter averaging has been performed here; nevertheless, the results are still qualitatively correct.

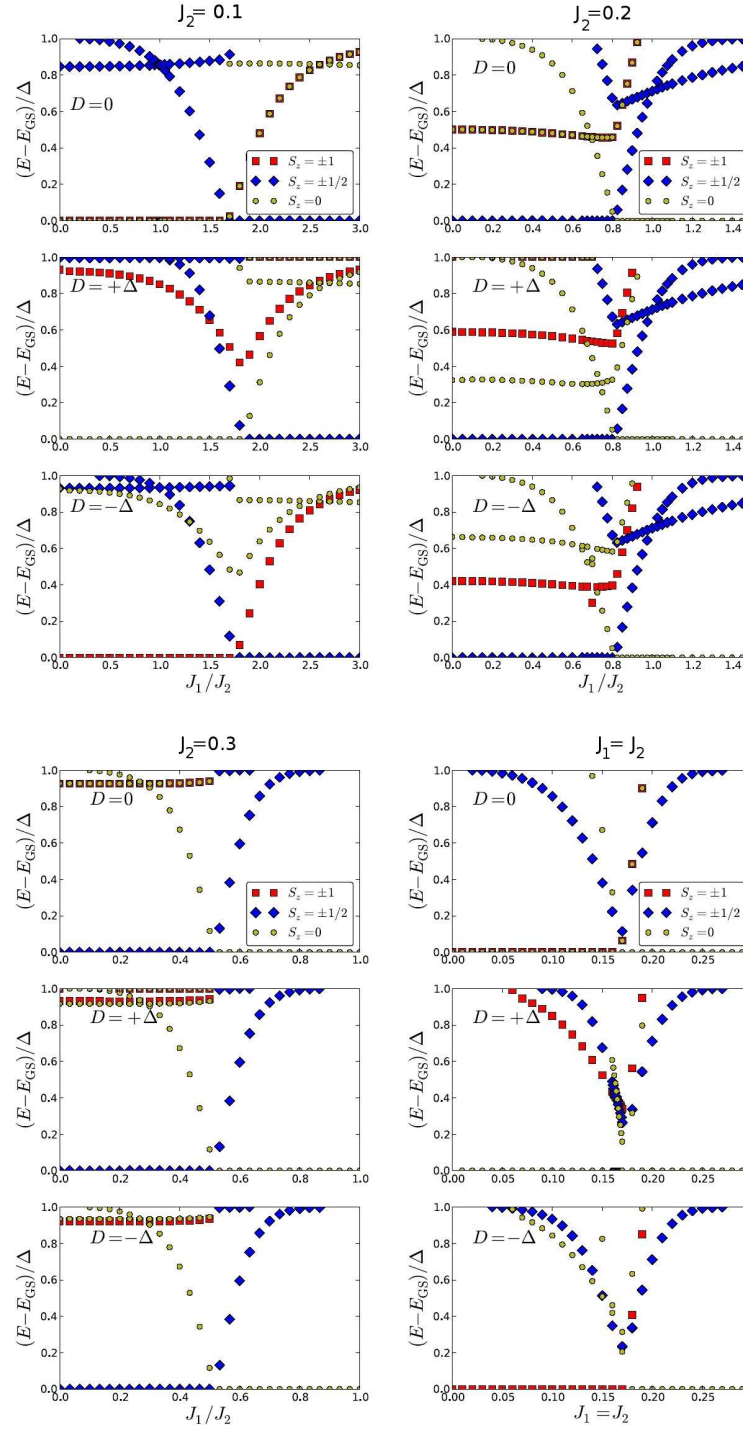


Figure 16: (Color online) Ground state and sub-gap many-particle excitations as a function of the parameters J_1 and J_2 for the two-channel $S_{\text{imp}} = 1$ Kondo model. The gap is $\Delta = 10^{-5}$. The results of these (and similar) calculations have been used to establish the schematic phase diagram for the $S_{\text{imp}} = 1$ case in Fig. 4 of the main text.

126601 (2006).

⁵⁷ G. González, M. N. Leuenberger, and E. R. Mucciolo, Phys. Rev. B **78**, 054445 (2008).

⁵⁸ O. Újsághy, A. Zawadowski, and B. L. Gyorffy, Phys. Rev. Lett. **76**, 2378 (1996).

⁵⁹ P. W. Anderson, Phys. Rev. **124**, 41 (1961).

⁶⁰ J. R. Schrieffer and D. C. Mattis, Phys. Rev. **140**, 1412 (1965).

⁶¹ J. R. Schrieffer and P. A. Wolff, Phys. Rev. **149**, 491 (1966).

⁶² B. Coqblin and J. R. Schrieffer, Phys. Rev. **185**, 847 (1969).

⁶³ G. Grüner and A. Zawadowski, Rep. Prog. Phys. **37**, 1497 (1974).

- ⁶⁴ P. W. Anderson, *Rev. Mod. Phys.* **50**, 191 (1978).
- ⁶⁵ A. C. Hewson, *The Kondo Problem to Heavy-Fermions* (Cambridge University Press, Cambridge, 1993).
- ⁶⁶ K. G. Wilson, *Rev. Mod. Phys.* **47**, 773 (1975).
- ⁶⁷ H. R. Krishna-murthy, J. W. Wilkins, and K. G. Wilson, *Phys. Rev. B* **21**, 1003 (1980).
- ⁶⁸ R. Bulla, T. Costi, and T. Pruschke, *Rev. Mod. Phys.* **80**, 395 (2008).
- ⁶⁹ W. C. Oliveira and L. N. Oliveira, *Phys. Rev. B* **49**, 11986 (1994).
- ⁷⁰ J. B. Silva, W. L. C. Lima, W. C. Oliveira, J. L. N. Mello, L. N. Oliveira, and J. W. Wilkins, *Phys. Rev. Lett.* **76**, 275 (1996).
- ⁷¹ C. A. Paula, M. F. Silva, and L. N. Oliveira, *Phys. Rev. B* **59**, 85 (1999).
- ⁷² V. L. Campo and L. N. Oliveira, *Phys. Rev. B* **72**, 104432 (2005).
- ⁷³ R. Žitko and T. Pruschke, *Phys. Rev. B* **79**, 085106 (2009).
- ⁷⁴ D. C. Mattis, *Phys. Rev. Lett.* **19**, 1478 (1968).
- ⁷⁵ D. M. Cragg and P. Lloyd, *J. Phys. C: Solid State Phys.* **12**, L215 (1979).
- ⁷⁶ P. Nozières and A. Blandin, *J. Physique* **41**, 193 (1980).
- ⁷⁷ D. M. Cragg, P. Lloyd, and P. Nozières, *J. Phys. C: Solid St. Phys.* **13**, 803 (1980).
- ⁷⁸ V. T. Rajan, J. H. Lowenstein, and N. Andrei, *Phys. Rev. Lett.* **49**, 497 (1982).
- ⁷⁹ P. D. Sacramento and P. Schlottmann, *Phys. Rev. B* **40**, 431 (1989).
- ⁸⁰ P. D. Sacramento and P. Schlottmann, *Phys. Rev. B* **43**, 13294 (1991).
- ⁸¹ D. L. Cox and A. Zawadowski, *Adv. Phys.* **47**, 599 (1998).
- ⁸² H. Suderow, E. Bascones, A. Izquierdo, F. Guinea, and S. Vieira, *Phys. Rev. B* **65**, 100519 (2002).
- ⁸³ J. G. Rodrigo, H. Suderow, S. Vieira, E. Bascones, and F. Guinea, *J. Phys. Cond. Matter* **16**, R1151 (2004).
- ⁸⁴ R. Meservey, P. M. Tedorow, and P. Fulde, *Phys. Rev. Lett.* **25**, 1270 (1970).
- ⁸⁵ R. Meservey, *Phys. Scr.* **38**, 272 (1988).
- ⁸⁶ W. Chen, T. Jamneala, V. Madhavan, and M. F. Crommie, *Phys. Rev. B* **60**, R8529 (1999).
- ⁸⁷ V. Madhavan, T. Jamneala, K. Nagaoka, W. Chen, J.-L. Li, S. G. Louie, and M. F. Crommie, *Phys. Rev. B* **66**, 212411 (2002).
- ⁸⁸ H. J. Lee, W. Ho, and M. Persson, *Phys. Rev. Lett.* **92**, 186802 (2004).
- ⁸⁹ C. F. Hirjibehedin, C. P. Lutz, and A. J. Heinrich, *Science* **312**, 1021 (2006).
- ⁹⁰ P. Wahl, P. Simon, L. Diekhöner, V. S. Stepanyuk, P. Bruno, M. A. Schneider, and K. Kern, *Phys. Rev. Lett.* **98**, 056601 (2007).
- ⁹¹ K. H. Lau and W. Kohn, *Surf. Sci.* **75**, 69 (1978).
- ⁹² V. S. Stepanyuk, W. Hergert, P. Rennert, K. Wildberger, R. Zeller, and P. H. Dederichs, *Phys. Rev. B* **54**, 14121 (1996).
- ⁹³ P. Hyldgaard and M. Persson, *J. Phys.: Condens. Matter* **12**, L13 (2000).
- ⁹⁴ V. S. Stepanyuk, A. N. Baranov, D. V. Tsvilin, W. Gergert, P. Bruno, N. Knorr, M. A. Schneider, and K. Kern, *Phys. Rev. B* **68**, 205410 (2003).
- ⁹⁵ T. O. Strandberg, C. M. Canali, and A. H. MacDonald, *Nature Materials* **6**, 648 (2007).
- ⁹⁶ M. E. Flatté and D. E. Reynolds, *Phys. Rev. B* **61**, 14810 (2000).
- ⁹⁷ D. K. Morr and N. A. Stavropoulos, *Phys. Rev. B* **67**, 020502(R) (2003).
- ⁹⁸ R. Žitko, M. Lee, R. López, R. Aguado, and M.-S. Choi, *Phys. Rev. Lett.* **105**, 116803 (2010).